IEEE Access
Multidisciplinary | Rapid Review | Open Access Journal

Received 23 February 2023, accepted 26 March 2023, date of publication 5 April 2023,
date of current version 4 December 2023.

Digital Object Identifier 10.1109/ACCESS.2023.3264947

RESEARCH ARTICLE

Research on Stellar Spectrum Simulation Method Based on Genetic Algorithm and Fuzzy PID Composite Control

YU ZHANG[1], YUEGANG FU[1,2,3], QIANG LIU[1], BIN ZHAO[1], JIAN ZHANG[1,2,3], GAOFEI SUN[1,2,3], SHITONG LIANG[4], LI WANG[4], AND JUN ZHONG[4]

[1]College of Optoelectronic Engineering, Changchun University of Science and Technology, Changchun 130022, China
[2]Jilin Province Optoelectronic Measurement and Control Instruments Engineering Research Center, Changchun 130022, China
[3]Key Laboratory of Optoelectronic Measurement and Control and Optical Information Transmission Technology, Ministry of Education, Changchun 130022, China
[4]Beijing Institute of Control Engineering, Beijing 100190, China

Corresponding author: Yuegang Fu (fuyg@cust.edu.cn)

This work was supported in part by the National Natural Science Foundation of China under Grant 62075019, and in part by the Science and Technology Development Program of Jilin Province under Grant 20200401046GX.

ABSTRACT For the current spectral simulation based on Digital Micromirror, the spectral simulation unit has different bias properties and nonlinear modulation, which leads to the lack of a spectral simulation method for multiple color temperature modulation. In this paper, a stellar spectrum simulation method based on Genetic Algorithm and fuzzy PID compound control was proposed. It analyzed the composition and working principle of the stellar spectrum simulation system, designed the corresponding matrix algorithm, studied the compound control spectral simulation algorithm of Genetic Algorithm and fuzzy PID, constructed a dual-input, three-output fuzzy PID controller architecture, and designed the Genetic Algorithm dual-optimized fuzzy PID control algorithm. In this research, an experimental platform was built to verify the generalization and simulation accuracy of the Genetic Algorithm and fuzzy PID compound control stellar spectrum simulation method based on the 2500K-10000K color temperature spectral curve as the target. The results indicated that the error of 2500K-10000K spectral simulation was between −2.91% and 2.94%, and the error of spectral curve area simulation was between −0.18% and 0.22%.As the smoothing of the star spectrum curves fails to verify the simulation ability of detailed characteristics such as peaks and troughs, the AM1.5 solar spectrum is taken as the simulation object, which verifies the performance of the star spectrum simulation method based on a genetic algorithm and a fuzzy PID integration.On this basis, the AM1.5 solar spectrum was taken as the simulation target to verify the ability to simulate detailed features such as wave peaks and troughs based on Genetic Algorithm with fuzzy PID compound control stellar spectrum simulation method. The results revealed that the accuracy of the single-point spectral simulation of AM1.5 solar spectrum is −5.76%, and the spectral curve area simulation error is 0.07%. The proposed method has the ability to simulate a wide range of color temperature targets with high accuracy. It has the ability to simulate detailed features such as wave peaks and troughs. It can provide a theoretical and technical basis for the ground calibration of the high-precision star sensor development.

INDEX TERMS Compound control, digital micromirror, fuzzy control, genetic algorithm, spectral simulation.

I. INTRODUCTION

At present, starlight navigation is an important technical means for navigation and attitude control of satellites,

The associate editor coordinating the review of this manuscript and approving it for publication was Chao Zuo.

spacecraft, space probes, and other types of spacecraft. Presently, most of them use star-sensitive star maps taken by star-sensitive instruments to obtain the position information of stars and star information to achieve attitude capture and measurement of spacecraft. As space technology develops and the space environment becomes more and more complex, depending on the star position and star information alone can no longer meet the new needs of current spacecraft navigation. Emerging navigation such as astronomical spectral velocimetry navigation by using spectral information has become the development trend of spacecraft navigation systems [1], [2]. Hence, the study of high-precision stellar spectrum ground simulation and calibration equipment to supplement the accuracy calibration and performance verification experimental conditions of emerging navigation methods of star-sensitive vehicles is valuable for the research and practical application to enhance the development level of star-sensitive vehicles and improve the accuracy of spacecraft autonomous navigation and control.

In nature, stellar spectrum simulation is a spectral modulation of a specific color temperature spectral profile. Numerous scholars worldwide have conducted many studies on this subject and have made some progress in stages. Originally, the spectral simulation used a single-filter target spectral simulation method, but this approach could not achieve multi-target spectral simulation, and the simulation accuracy was low [3]. Thus, in 2005, the Bialystok Technical University in Poland achieved output spectral modulation with a single-point spectral simulation error of about 30% by selecting the LED spectral type and controlling the LED energy [4], [5]. In 2016, Guang-qiang et al. performed simulations of the stellar spectrum using an array of 25 LEDs with different central wavelengths, covering the spectral range 365 nm-940 nm [6]. However, as the limitation of the central wavelength selection of LEDs by the technology level, the absence of certain wavelengths can lead to a simulation dead zone in the spectral simulation of broad-spectrum targets. In 2017, Davis and Cogdell, established a simulation database of LED spectral distribution functions and implemented a solar spectral simulation in the visible range using monochromatic LEDs to compensate for white LEDs based on the least squares principle [7]. While the accuracy of the spectral simulation of such methods is gradually improving, the limitation of LED band types and the poor fitting of the LED spectral distribution function limits the further improvement of the accuracy of the spectral simulation of such methods.

Along with the development of spatial light modulation technology, the further subdivision of the spectral simulation unit has become possible, leading to the research direction of spectral simulation using the dispersive system with a digital micromirror device (DMD). Among them, Brown et al. at NIST in 2010 constructed a spectrally tunable irradiance standard light source system, which uses a combination of xenon, Bromine tungsten lamp, and LED light sources as external inputs, modulated by a light engine and fed into an integrating sphere, as a way to achieve a specific spectral simulation [8]. In 2016, Luo et al. designed a spectrally programmable light source based on a Digital Micromirror device (DMD) for the decomposition of broad-spectrum beams to enable the analysis of broad-band spectra [9]. In 2018, Wang and Li developed a dual-grating spectrally tunable light source based on the Ebert-Fastie structure using DMD to achieve narrow-band spectral output with output monochromatic optical uncertainties of 4.68% at 450 nm, 1.54% at 550 nm, and 1.48% at 654.6 nm [10]. In 2021, Xu et al. used DMD to achieve three typical stellar color temperatures in the spectral range of 500 nm-900 nm, 3000 K, 5000 K, and 7000 K, with color temperature spectral simulation accuracy better than 5.2% [11]. In 2022, Liang Jing et al. proposed a spectral simulation method based on the least-squares method based on the residual-free homogeneous mechanism [12] and a spectral correction method based on the maximum simulation error [13] for the spectral simulation of 2700 K color temperature, and the spectral simulation errors were $\pm 5.7\%$ and $\pm 6.2\%$, respectively. However, the applicability of these two methods was only verified for 2700 K color temperature spectral simulation, and there is a lack of research on efficient spectral simulation methods for DMD-based spectral simulation systems with high accuracy and multiple color temperatures.

The advanced principles of the DMD spectral simulation method enable the spectrum simulation accuracy to be improved compared to the LED spectral simulation method. However, it was found that there is a region of spectral overlap between the spectral simulator units and the non-linear energy modulation of each row of PMD micromirror arrays [10]. As a result, the error of control methods such as traditional PID and classical genetic algorithms increases in the case of multiple correlations with independent variables [14]. Although fuzzy PID can alleviate the above problems to a certain extent [15], problems such as imitation target limitations and modulation lack of fit will emerge in the process of multi-target spectral simulation due to the limitations of a priori [16].

Therefore, a star spectrum simulation method based on a genetic algorithm and fuzzy PID compound control is proposed in this thesis based on DMD spectrum simulation. The combination of the genetic algorithm and the fuzzy PID controller eliminates the limitation of the expert experience in the fuzzy PID on the performance of spectral simulation, to realize the high-precision spectral simulation with generalization.

II. ESTABLISHMENT OF STELLAR SPECTRUM SIMULATION SYSTEM WITH SPECTRAL SIMULATION MATRIX ALGORITHM

A. THE STELLAR SPECTRUM SIMULATION SYSTEM COMPOSITION AND GENERAL STRUCTURE

The stellar spectrum simulation system mainly consists of the broad-spectrum light source, Czerny-Turner dispersive

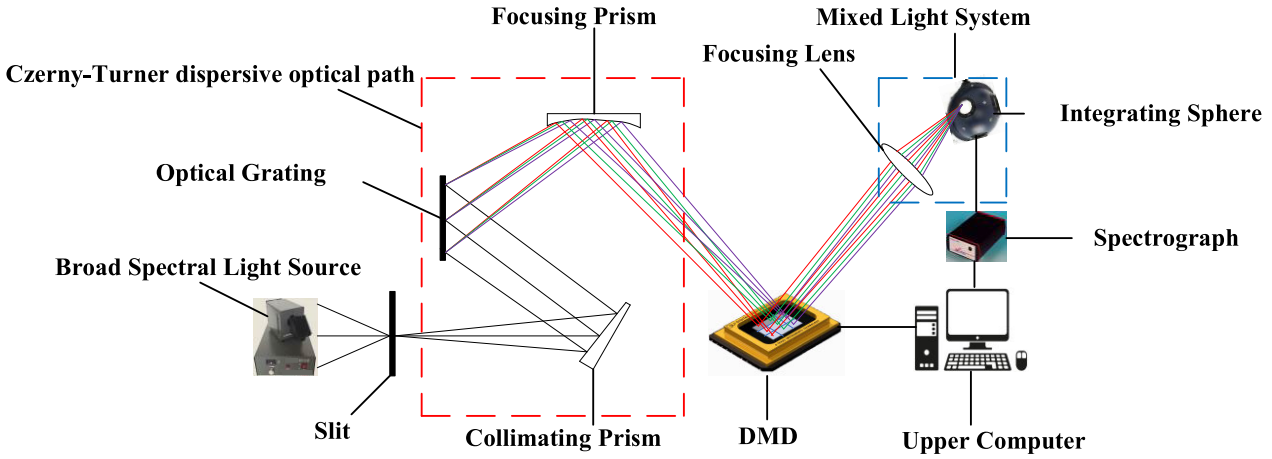

FIGURE 1. Block diagram of the stellar spectrum simulation system.

optical path, DMD, mixing system, spectrometer, upper computer, etc. The operating optical path diagram of the system and the built experimental platform are shown in Figure 1.

The broad-spectrum light source emits a broad-spectrum beam, which enters the Czerny-Turner dispersive path through the slit. Then it shines on the DMD after dividing the Czerny-Turner dispersive path, forming a series of spectral simulation units with different peak wavelengths. By controlling the switching state of the array micro-mirrors of the DMD, the spectral simulation units of different proportions are reflected to the focusing lens and converge into the integrating sphere to mix the light, thus realizing the wide band stellar spectrum simulation. The spectrometer detects the curve distribution of the spectrum in the integrating sphere through optical fiber and transmits it to the host computer. Based on the obtained feedback information, the host computer uses the spectral simulation algorithm to adjust the switching state of the DMD array micromirror to achieve high-precision modulation of the target stellar spectrum.

B. DMD-BASED SPECTRAL SIMULATION MATRIX ALGORITHM

Based on the principle of spectral superposition [17] and the operating mechanism of DMD [18], the target stellar spectrum curve information is actually the superposition of the radiation flux reflected into the integrating sphere from the DMD micromirror array, so the current stellar spectrum curve can be discretized and converted from the two-dimensional curve form to the two-dimensional matrix form. The DMD-based stellar spectrum simulation model can be established through the matrix algorithm. For the sake of discussion, the following equations were discussed with the number of DMD rows as n, the number of different peak wavelength spectral simulation units as m, and the peak wavelength as $\lambda_1, \lambda_2 \cdots \lambda_m$.

1) TARGET SPECTRAL CURVE MATRIX

Let the radiation flux corresponding to different wavelengths of the target spectral curve be $T(\lambda_i)$, for the matrix form T of the target spectrum can be expressed as

$$T = \begin{bmatrix} \phi_{11} & \phi_{12} & \cdots & \phi_{1m} \\ \phi_{21} & \phi_{22} & \cdots & \phi_{2m} \\ \vdots & \vdots & \ddots & \vdots \\ \phi_{m1} & \phi_{m2} & \cdots & \phi_{mm} \end{bmatrix} \tag{1}$$

Refer to "(1)," Where ϕ_{ij} is the luminous flux transferred into the integrating sphere by the numerical micromirror corresponding to the DMD. At this point, there is

$$\begin{aligned} &\textstyle\sum_{i=1}^{n} \phi_{i1} : \sum_{i=1}^{i} \phi_{i2} \cdots\cdots \sum_{i=1}^{n} \phi_{im} \\ &\quad = T(\lambda_1) : T(\lambda_2) \cdots\cdots T(\lambda_m) \end{aligned} \tag{2}$$

2) DMD SPECTRAL MODULATION MATRIX

The elements in the DMD spectral modulation matrix represent the operating state of the micromirror array. Let the DMD spectral modulation matrix be D_{mn}, and the DMD operating matrix be

$$D = \begin{bmatrix} D_{11} & D_{12} & \cdots & D_{1m} \\ D_{21} & D_{22} & \cdots & D_{2m} \\ \vdots & \vdots & \ddots & \vdots \\ D_{n1} & D_{n2} & \cdots & D_{nm} \end{bmatrix} \tag{3}$$

Refer to "(3)," $D_{nm} = 1$ represents DMD array micromirror open, $D_{nm} = 0$ represents DMD array micromirror closed.

3) SPECTRAL MODULATION WEIGHT MATRIX

Since the spectral radiation intensity at different wavelengths of the spectral curve of a broad-spectrum light source is recorded as $S(\lambda_i)$, there is a proportional relationship between the radiation fluxes modulated by the spectral simulation units at different peak wavelengths after dispersion by the Czerny-Turner dispersion path and the proportional

relationship is approximated by the ratio of the spectral radiation intensities at different wavelengths on the spectral curve of the broad spectrum, which is recorded as $P_{\lambda_1} : P_{\lambda_2} \cdots\cdots P_{\lambda_m} = S(\lambda_1) : S(\lambda_2) \cdots\cdots S(\lambda_m)$.

Therefore, the spectral modulation weight matrix K is established as

$$D = \begin{bmatrix} K_{11} & K_{12} & \cdots & K_{1m} \\ K_{21} & K_{22} & \cdots & K_{2m} \\ \vdots & \vdots & \ddots & \vdots \\ K_{n1} & K_{n2} & \cdots & K_{nm} \end{bmatrix} \tag{4}$$

Refer to "(4)," Where K_{nm} denotes the radiation flux that can be modulated on one array micromirror of the DMD after normalization, at which point there is

$$\begin{aligned} &\sum_{i=1}^{n} K_{i1} : \sum_{i=1}^{n} K_{i2} \cdots\cdots \sum_{i=1}^{n} K_{im} \\ &\quad = P_{\lambda 1} : P_{\lambda_2} \cdots\cdots P_{\lambda_m} \end{aligned} \tag{5}$$

4) TARGET SPECTRAL SIMULATION ALGORITHM

The target spectral curve matrix, DMD spectral modulation matrix, and spectral modulation weight matrix are used to build the DMD-based spectral simulation matrix by using the target spectral simulation algorithm. The target spectrum simulation algorithm is

$$T = D \cdot K = \begin{bmatrix} D_{11}K_{11} & \cdots & D_{1m}K_{1m} \\ \vdots & \ddots & \vdots \\ D_{n1}K_{n1} & \cdots & D_{nm}K_{nm} \end{bmatrix} \tag{6}$$

III. COMPOUND CONTROL SPECTRAL SIMULATION ALGORITHM BASED ON GENETIC ALGORITHM AND FUZZY PID

The matrix algorithm of DMD-based spectral simulation shows that the spectral curve band of the broad-spectrum light source in the modulation process can have a great impact on the spectral simulation. At the same time, due to the nature of the Czerny-Turner dispersive optical path [19], the direct ratio of the column elements in the spectral modulation weight matrix K is difficult to grasp accurately. For the traditional PID control of the spectral simulation method can not handle the above situation, so this paper adopts the fuzzy PID control, which can overcome the uncertainty and non-linearity of the controlled object to modulate the target spectral curve. Nevertheless, since the affiliation function and fuzzy rules of fuzzy PID control developed by humans are highly subjective [20], for this reason Genetic Algorithm with the excellent global seeking ability and strong robustness and adaptability is used to double optimize the affiliation function and fuzzy rules of fuzzy PID control to avoid the limitation of spectral simulation performance in fuzzy PID and improve the control performance and spectral simulation accuracy of fuzzy PID controller.

A. DESIGN OF FUZZY PID CONTROLLER

1) DETERMINE THE INPUT AND OUTPUT VARIABLES DETERMINED

A two-input, three-output fuzzy PID controller structure is constructed with the spectral intensity deviation E_λ and deviation rate $E_{c\lambda}$corresponding to the spectral wavelength λ as input variables and the proportional coefficient increment ΔK_p, integral coefficient increment ΔK_i, and differential coefficient increment ΔK_d as output variables. E_λ and $E_{c\lambda}$ are expressed as

$$\begin{aligned} E_\lambda &= I(\lambda) - I_0(\lambda) \\ E_{c\lambda} &= \frac{dE_{c\lambda}}{dt} = \frac{[E_\lambda(n) - E_\lambda(n-1)]}{T} \end{aligned} \tag{7}$$

Refer to "(7)," Where $I(\lambda)$ and $I_0(\lambda)$ are the simulated spectral intensity at wavelength λ and the target spectral intensity, $E_\lambda(n)$ is the spectral intensity deviation of the current state and $E_\lambda(n-1)$ is the spectral intensity deviation of the previous state.

2) AFFILIATION FUNCTION SELECTION AND FUZZY RULE FORMULATION

Since the affiliation function and the fuzzy rule will be double optimized using Genetic Algorithm subsequently, the input and output variables are described by the five linguistic variable values of the fuzzy set {NB(negative greater), NS(negative smaller), ZR(zero), PS(positive smaller), PB(positive greater)}. While the domain area covered by the fuzzy subset affiliation function directly affects the performance of the fuzzy controller, the shape of the fuzzy affiliation function, such as triangular, Gaussian, and bell-shaped, does not have a great impact on it [21]. Hence, to facilitate the optimization of the affiliation function, the affiliation function uses a triangular function shape, The three initial triangle affiliation functions are shown in Figure 2.

The expression of the triangular affiliation function is shown in equation (8)-(10).

$$A(x) = \begin{cases} 1, & x \le a \\ \dfrac{b-x}{b-a}, & a \le x \le b \\ 0, & x \ge b \end{cases} \tag{8}$$

$$A(x) = \begin{cases} \dfrac{x-a}{b-a}, & a \le x \le b \\ \dfrac{c-x}{c-b}, & b \le x \le c \\ 0, & x \ge c \end{cases} \tag{9}$$

$$A(x) = \begin{cases} 0, & x \le b \\ \dfrac{x-b}{c-b}, & b \le x \le c \\ 1, & x \ge c \end{cases} \tag{10}$$

and the unoptimized E, E_c, K_p, K_i, K_d affiliation function is the same affiliation function. The unoptimized affiliation function curve is shown in Figure 3.

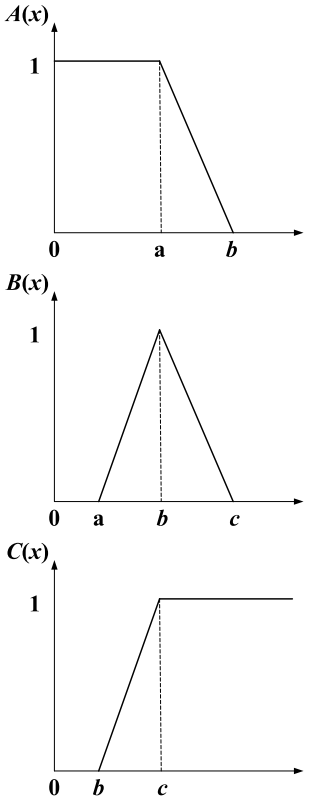

FIGURE 2. Initial affiliation function graph.

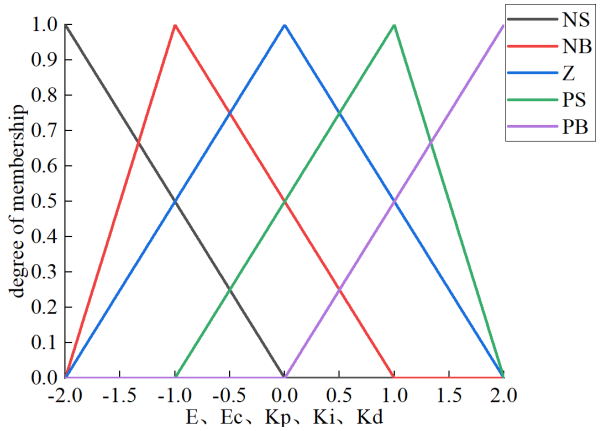

FIGURE 3. Membership function curve of input and output.

Likewise, since the fuzzy rules will be optimized by Genetic Algorithm subsequently, the fuzzy rules for initial K_p, K_i and K_d developed according to the fuzzy rule selection principle are shown in Table 1.

3) DEFUZZIFICATION

The fuzzy inference results in fuzzy quantities, while exact quantities are required in the actual control process. Therefore, this study adopted the center of gravity method [22] for defuzzification operation, as the final output value of fuzzy

TABLE 1. Fuzzy pid control rules (K_p. K_i. K_d).

E_λ \ $E_{c\lambda}$	NB	NS	ZR	PS	PB
NB	NS	ZR	PS	PS	ZR
NS	ZR	PS	PS	ZR	NS
ZR	ZR	ZR	ZR	NS	NS
PS	PS	PS	NS	NB	NB
PB	PS	PS	NS	NB	NB

inference is expressed as

$$\begin{aligned}\Delta K_p &= \frac{\sum \mu_j(u_p)\cdot u_p}{\sum \mu_j(u_p)}\\ \Delta K_i &= \frac{\sum \mu_j(u_i)\cdot u_i}{\sum \mu_j(u_i)}\\ \Delta K_d &= \frac{\sum \mu_j(u_d)\cdot u_d}{\sum \mu_j(u_d)}\end{aligned} \tag{11}$$

Refer to "(11)," ΔK_p, ΔK_i, $\Delta K_d$are the exact values of the fuzzy controller output change quantity solution fuzzy, u_p, u_i, u_d are the values in the domain of fuzzy control quantity theory, $\mu_j(u_p)$, $\mu_j(u_i)$, $\mu_j(u_d)$ are the affiliation degrees at u_p, u_i, u_d.

B. DESIGN OF GENETIC ALGORITHM DUAL OPTIMIZED FUZZY PID CONTROL ALGORITHM

The basic elements of the Genetic Algorithm dual-optimal fuzzy control algorithm are mainly coding method formulation, initial population generation, fitness function selection, and genetic operation operator determination.

1) FORMULATION OF CODING METHODS

This paper adopted a hybrid coding approach. That is, the fuzzy rules are expressed in decimal, and the affiliation parameters are expressed in floating point numbers to reduce the optimization time and decrease the complexity of coding. Among them, the fuzzy rules {NB, NS, Z, PS, PB} are coded as {1,2,3,4,5}, and 0 is used to indicate the absence of fuzzy rules. For each group of affiliation, each affiliation function vertex is chosen as the optimization parameter, i.e., there are 13 affiliation function parameters to be optimized in each group. At this point, the affiliation function code can be written as $n_1n_2n_3\cdots n_{63}n_{64}n_{65}$, then, the fuzzy rule and the affiliation function are jointly coded as a 140-bit length mixed code.

2) GENERATION OF INITIAL POPULATIONS

The initial population is generated in a procedural random way, and the generation rules are:

1. All individuals in the generated random initial population matrix $Z_0 = \left[z_0^1, z_0^2, z_0^3\cdots z_0^n\right]^T$ are not identical to each other. That is, for any $i \neq j(i,j \in \{1,2,\cdots n\})$, there is $z_0^i \neq z_0^j$;

2. These two individuals are not identical at the same gene locus. That is, for any $i \neq j(i, j \in \{1, 2, \cdots n\}, k \in \{1, 2, \cdots p\})$, there is $z_0^i k \neq z_0^j k$.

3. In the meantime, set the evolutionary generation timer $G_{\text{en}} = 0$ and set the maximum evolutionary generation G, then the termination condition is $G_{\text{en}} = G$.

3) SELECTION OF THE FITNESS FUNCTION

In accordance with the rules for selecting the fitness function and the way of fitting the spectral distribution function for evaluation, the fitness function is chosen as:

$$j = \sqrt{\sum [y_k(\lambda) - y(\lambda)]^2 / n} \tag{12}$$

Refer to "(12)," $y_k(\lambda)$ is the fuzzy PID output node value, $y(\lambda)$ is the desired output value.

4) DETERMINATION OF THE GENETIC OPERATOR

The genetic operators mainly include selection, crossover, and variation operators.

1. Selection operator: the roulette wheel method is used. That is, the assignment is based on the preponderance of fitness, and the probability of inheriting offspring is

$$P_i = \frac{f_k}{\sum_{l=1}^{S_p} f_l} \tag{13}$$

Refer to "(13)," S_p is the population size. f_k is the fitness of the individual k. l is the number of counts different from i.

2. Crossover operator: The crossover operator uses the method of comparing the size of random numbers to determine whether the readings need to be crossed, and the crossover operation criterion is:

$$f(P_{ct}) = \begin{cases} 1, P_{ct} \leq P_c \\ 0, P_{ct} > P_c \end{cases} \tag{14}$$

Refer to "(14)," Where P_{ct} is the random number generated in this round, and P_m is the crossover probability.

The real number crossover method is used for the crossover operation to ensure randomness, and the equation is

$$\begin{aligned} G_{ij} &= G_{ij} \times (1 - b) + G_{ij} \times b \\ G_{kj} &= G_{kj} \times (1 - b) + G_{kj} \times b \end{aligned} \tag{15}$$

Refer to "(15)," Where G_{ij} denotes the j-th chromosome of the i-th individual and b is a random number with a value range of 0 to 1.

3. Variation operator: The variation operator uses the method of comparing the size of random numbers to determine whether the reading needs variation operation, and the variation operation criterion is:

$$f(P_{mt}) = \begin{cases} 1, P_{ct \leq P_m} \\ 0, P_{ct > P_m} \end{cases} \tag{16}$$

Refer to "(16)," Where P_{mt} is the random number generated in this round, and P_m is the variance probability.

The variation operation equation is

$$G_{ij} = (G_{\max} - G_{\min}) \times b \times G_{\max} \tag{17}$$

Refer to "(17)," Where G_{ij} denotes the j-th chromosome of the i-th individual, b is a random number with a value range of 0 to 1, $G_{\max}$ is the maximum value of a single chromosome desirable for a single sample, and $G_{\min}$ is the minimum value of a single chromosome desirable for a single sample.

The Genetic Algorithm dual-optimized fuzzy PID control algorithm flow is shown in Figure 4.

IV. MATHEMATICAL EXPERIMENTS AND ANALYSIS

As shown in Figure 5, it is shown that the stellar spectrum simulation experimental platform is built for the selected broad spectrum light source, Czerny-Turner dispersive optical path, DMD, integrating sphere, and fiber optic spectrometer. The main parameters of the experimental platform are shown in Table 2.

A. ANALYSIS OF FUZZY RULES AND AFFILIATION FUNCTIONS BEFORE AND AFTER OPTIMIZATION

In order to verify the generalizability of the Genetic Algorithm and the fuzzy PID based found control spectral simulation algorithm, taking into account the spectral curve trend, three typical characteristic target spectral shapes in the wavelength range of 400 nm to 800 nm are firstly chosen. Simulation curve shapes of 2500K, 5000K, and 10000k are used as the simulated target spectra. After iterative optimization, the fuzzy rules and affiliation functions of the compound control spectral simulation algorithm based on the Genetic Algorithm with fuzzy PID are obtained.

The initialization setting parameters of the Genetic Algorithm dual optimized fuzzy controller are shown in Table 3. The optimized affiliation function is shown in Figure 5.

The K_p, K_i, and K_d fuzzy rules after iterative optimization are shown in Table 4.

According to Table 4, after the Genetic Algorithm optimization, the K_p takes a larger value at the beginning of the regulation to improve the response speed. In the middle of regulation, a smaller value is taken to make the system have a smaller overshoot and ensure a certain response speed. In the later stage of regulation, the value is increased to reduce the static error and improve the control accuracy. In the early stage of regulation, to prevent integration saturation, the value of K_i is small or even zero. In the middle of regulation, to avoid affecting the stability, the value is moderate, while in the late regulation, the value is increased to enhance the integration effect and reduce the static regulation difference. The value of K_d is larger at the beginning of regulation to obtain smaller or even avoid overshoot, smaller at the middle of regulation, and smaller at the end to reduce the braking effect of the controlled process and thus compensate for the

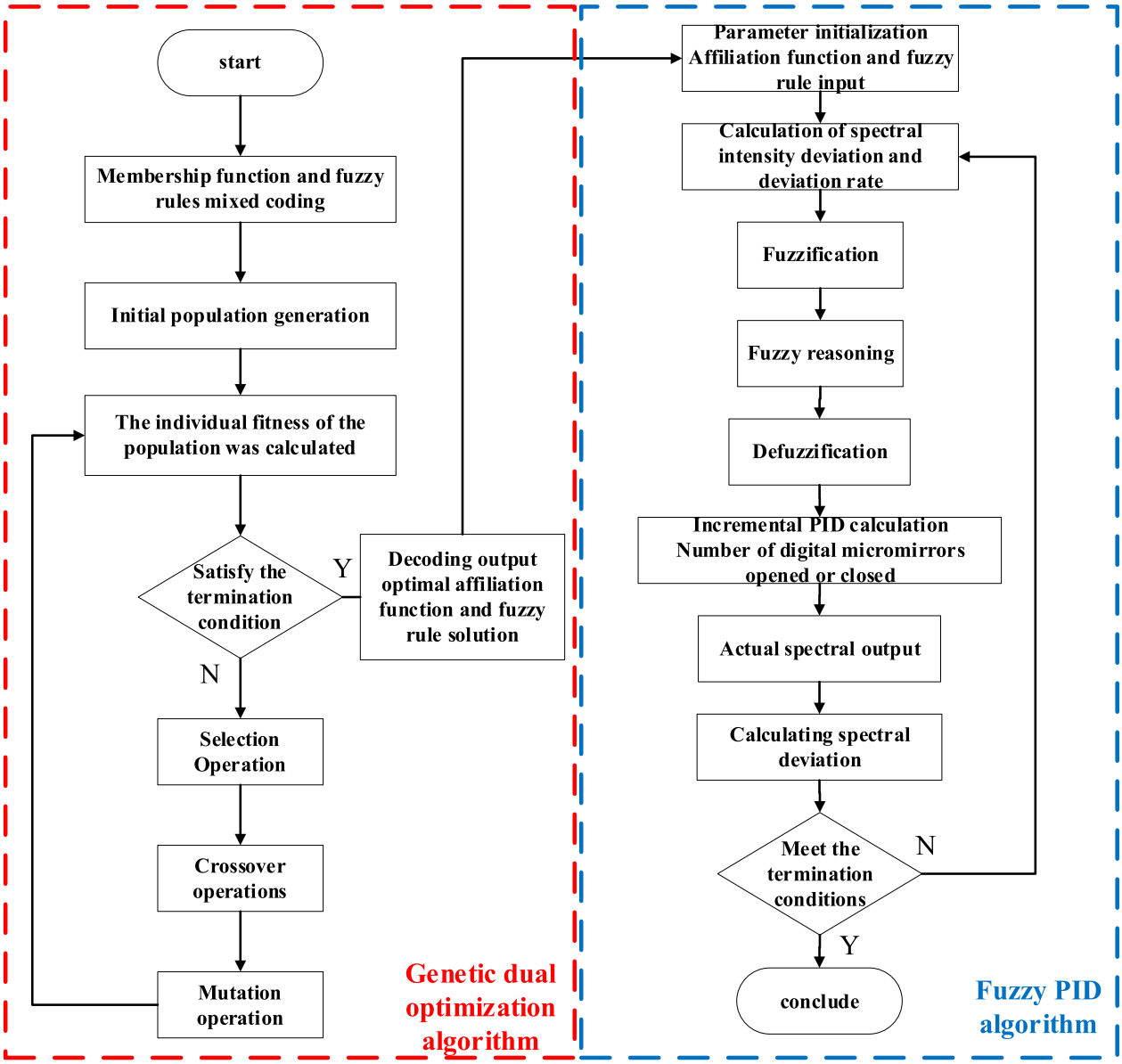

FIGURE 4. Genetic Algorithm dual-optimized fuzzy PID control algorithm flow chart.

prolonged regulation time caused by the larger value at the beginning of regulation.

A comparison of the affiliation function curves before and after the Genetic Algorithm optimization is shown in Figure 6.

The solid part of the figure shows the affiliation function before optimization, and the dashed part shows the affiliation function curve after optimization. According to Fig. 5, it can be seen that the optimized affiliation functions of E_λ, $E_{c\lambda}$, K_p, K_i and K_d adopt triangular function shapes with changed vertices, and the area of the thesis domain covered by the corresponding set of affiliation functions also changes.

B. ABSOLUTE COLOR TEMPERATURE SPECTRAL SIMULATION EXPERIMENT

In consideration of the evaluation of the details and the overall performance of the spectral simulation, two methods were chosen to evaluate the effect of the spectral simulation: the single-point spectral simulation error and the spectral curve area simulation error. The single-point spectral simulation error is the relative error of the simulated spectral radiation intensity I'_λ at a certain wavelength to the target radiation intensity I_λ, and the specific equation is $E_\lambda = \frac{I'_\lambda - I_\lambda}{I_\lambda}$. The spectral curve area simulation error is the relative error of the simulated spectral curve area A'_S relative to the target spectral

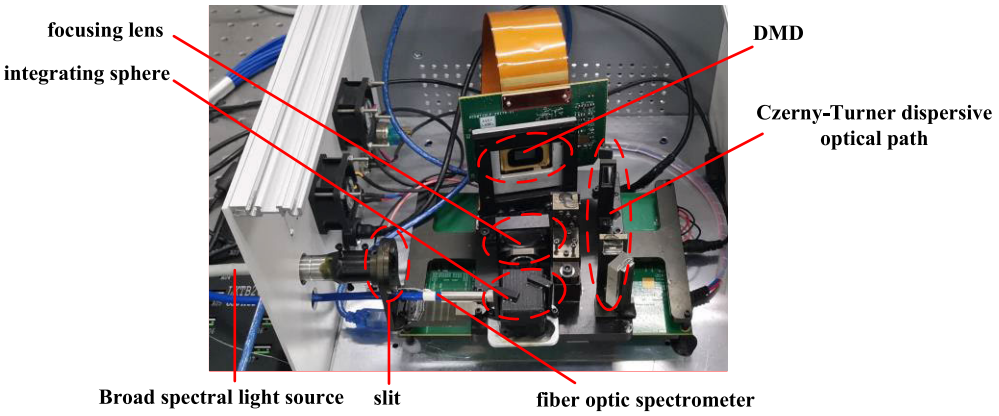

FIGURE 5. Experimental platform.

TABLE 2. Test bench parameters.

Index		Parameter
Broad spectral light source	Spectral range	200nm-2500nm
Czerny-Turner dispersive optical path	Spectral range	400nm-800nm
	Spectral resolution	0.5nm
DMD	resolution	1920x1080
Integrating sphere	Spectral range	250nm-2500nm
	reflectance	>95%
Optical spectrometer	Spectral range	200nm-1160nm
	Spectral resolution	0.5nm

curve area A_S in a wide wavelength band, and the specific equation is $E_S = \frac{A'_S - A_S}{A_S}$.

After several iterations of optimization in Section IV-A, the simulated results of 2500K, 5000K, and 11000k color temperature spectral curves with single point spectral simulation error results are shown in Figure 7.

According to the Figure 7, it can be seen that the spectral curves with different distribution trends have good simulation results with little correlation with the trends of the spectral curves. The maximum single point spectral simulation errors for 2500 K, 5000 K, and 10000 K and the corresponding wavelength and spectral curve area simulation errors are shown in Table 5.

The results of the individual spectral simulation errors and spectral curve area simulation errors for the absolute color temperature range of 2500K-10000K (500K interval) are shown in Figure 7.

According to Figure 8, it can be concluded that the error of single-point spectral simulation from 2500K-10000K is between −2.91% and 2.94%, and the error of spectral curve area simulation is between -0.18% and 0.22%, which indicates that the compound control based on Genetic Algorithm with fuzzy PID The spectral simulation algorithm has a good simulation effect in the absolute color temperature range of 2500K-10000K.

TABLE 3. Initialization setup parameters for the dual-optimized fuzzy controller of the genetic algorithm.

Name	Parameter
Initial population size	200
Maximum Generation	200
crossover probability	0.7
mutation probability	0.005
Spectral simulation error	3%

TABLE 4. K_p fuzzy rules after genetic algorithm optimization.

		$E_{c\lambda}$				
	E_λ	NB	NS	ZR	PS	PB
K_p	NB	PB	PB	ZR	PS	ZR
	NS	PB	PS	PS	ZR	NS
	ZR	ZR	PS	ZR	NS	NS
	PS	PS	ZR	NS	NB	NB
	PB	ZR	NS	NS	NB	NB
	E_λ	NB	NS	ZR	PS	PB
K_i	NB	PB	PB	ZR	PS	ZR
	NS	PB	PS	PS	ZR	NS
	ZR	ZR	PS	ZR	NS	NS
	PS	PS	ZR	NS	NB	NB
	PB	ZR	NS	NS	NB	NB
	E_λ	NB	NS	ZR	PS	PB
K_d	NB	PB	PB	ZR	PS	ZR
	NS	PB	PS	PS	ZR	NS
	ZR	ZR	PS	ZR	NS	NS
	PS	PS	ZR	NS	NB	NB
	PB	ZR	NS	NS	NB	NB
	NB	PB	PB	ZR	PS	ZR

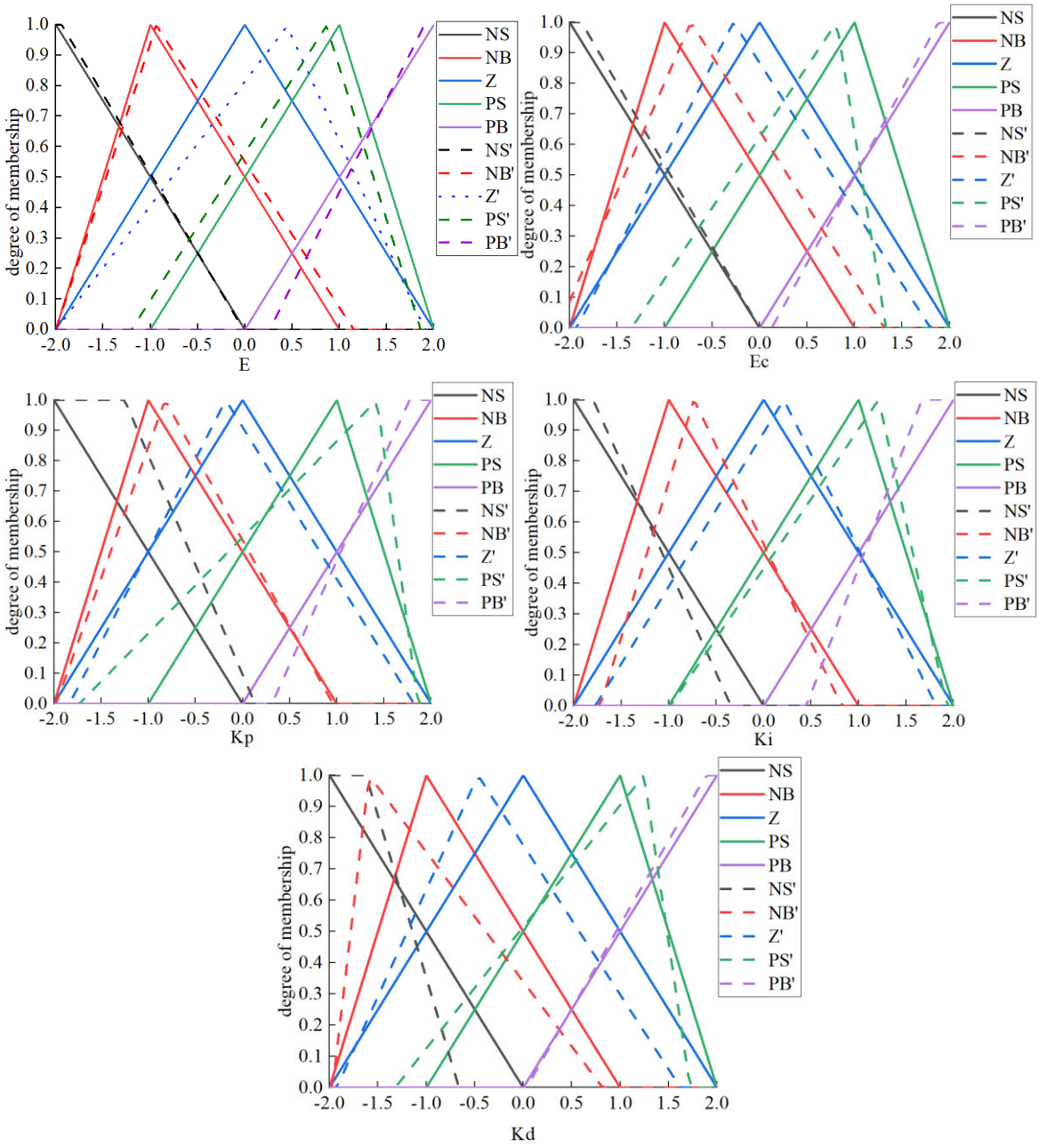

FIGURE 6. Affiliation function curve after optimization.

C. AM 1.5 SOLAR SPECTRAL SIMULATION EXPERIMENT

According to the absolute color temperature spectral simulation experiments, it is known that the compound control spectral simulation algorithm based on Genetic Algorithm with fuzzy PID has good generalization and simulation accuracy for smoothing the spectral curve. In consideration of other special cases of stellar spectrum simulation, therefore, based on the optimized fuzzy rules and affiliation functions, the AM1.5 solar spectrum with detailed features such as wave peaks and troughs is used as the simulation target to verify the ability of the compound control spectral based on Genetic Algorithm with fuzzy PID The simulation results of the AM 1.5 solar spectrum are shown in Figure 9.

It can be seen from Figure 9 that the single-point spectral simulation error can still be maintained within ±3% in the smoother region of the AM3.5 solar spectrum. However, in the case of large slope abrupt changes in the shape of the spectral curve, the single-point spectral simulation error can only converge to within ±6%, especially in the three bands from 416 nm to 450 nm, 670 nm to 743 nm and 757 nm to 772 nm. The maximum single-point spectral simulation error from 400 nm to 800 nm in the AM1.5 solar spectrum

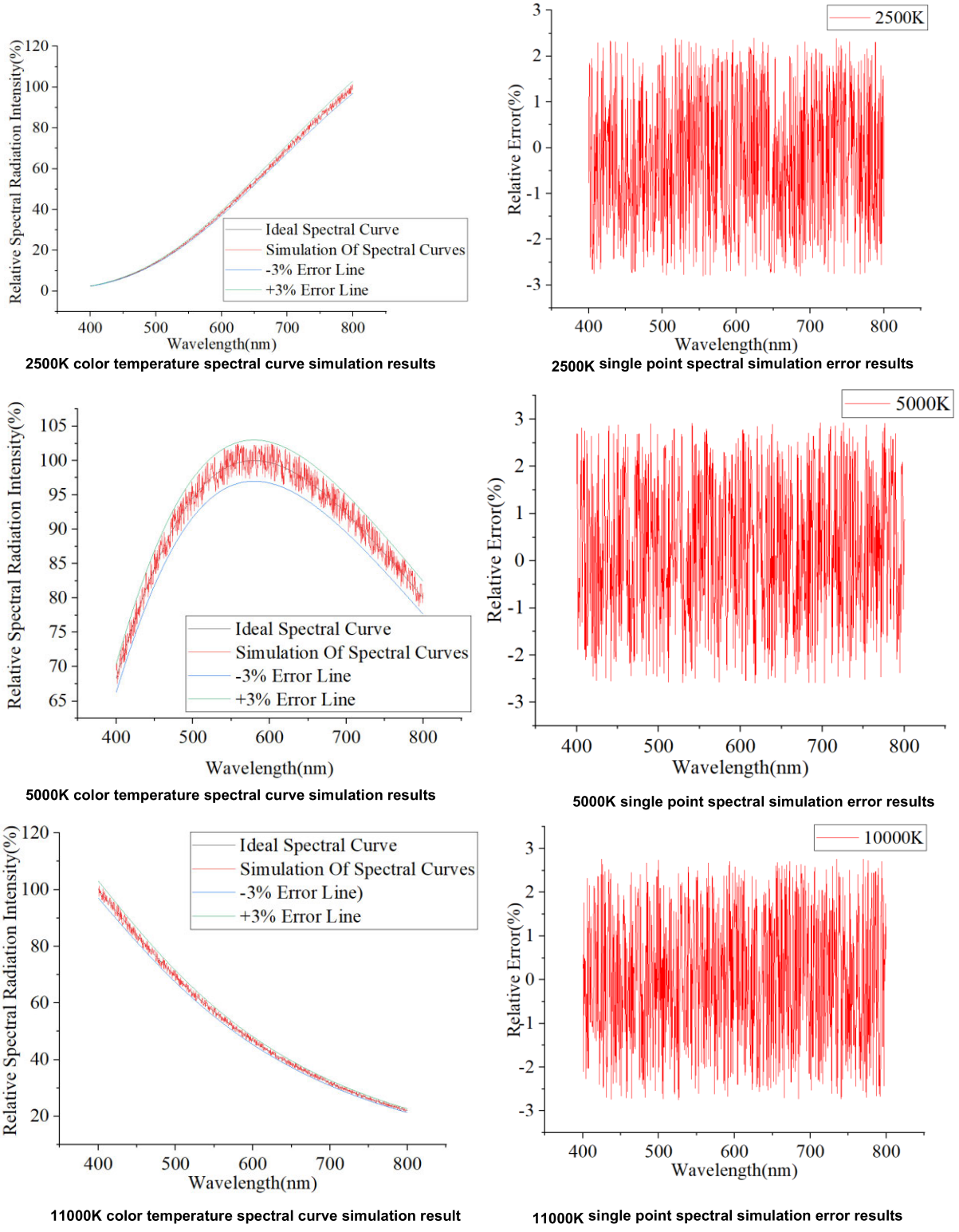

FIGURE 7. 2500K, 5000K, 10000K experimental diagram.

is −5.76%, and the spectral curve area simulation error at this point is 0.07%. It can be seen that although the single point spectral simulation error of AM1.5 solar spectrum has a large difference relative to the absolute color temperature spectral curve from 2500K to 10000K. Nevertheless, the spectral curve area simulation error is very close to that of

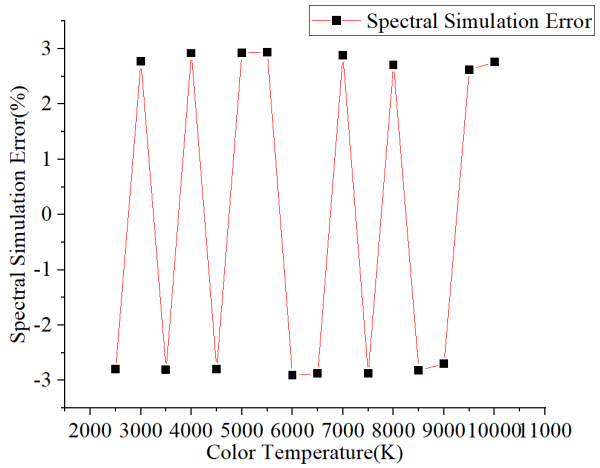

FIGURE 8. 2500-10000K color temperature spectral simulation error chart.

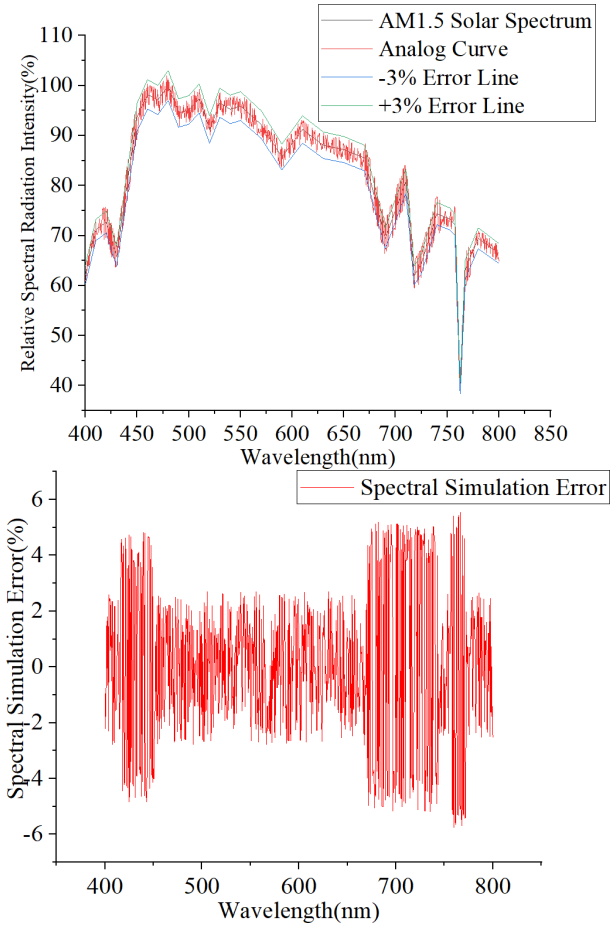

FIGURE 9. AM1.5 solar spectrum.

the absolute color temperature from 2000 K to 10,000 K. This indicates that the compound control spectral simulation algorithm based on Genetic Algorithm with fuzzy PID still has good performance for spectral curves with detailed features such as peaks and valleys without the need for very obvious spectral feature peaks simulation.

TABLE 5. Maximum single point spectral simulation errors for 2500K, 5000K, and 10000K and the corresponding wavelength and spectral curve area simulation errors.

Color temperature	Maximum single point spectral simulation error	Wavelength	Spectral curve area simulation error
2500K	-2.8%	556nm	0.18%
5000K	2.93%	697.5nm	0.22%
10000K	2.76%	424.5nm	0.02%

V. CONCLUSION

In response to the problems of multiple correlations among spectral simulation units and nonlinearity of radiation weights among image elements in the current DMD-based spectral simulation, which lead to the limitations and modulation underfitting of traditional PID control and other spectral simulation methods in multiple target spectral simulations, this paper proposed a stellar spectral simulation method based on genetic algorithm and fuzzy PID composite control.

This paper analyzed the composition and working principle of the stellar spectral simulation system; established the matrix algorithm of spectral simulation based on DMD; constructed a two-input, three-output fuzzy PID controller consisting of spectral intensity deviation and deviation rate and proportional coefficient, integral coefficient and differential coefficient, selected the affiliation function of triangular function shape, formulated the initial fuzzy rules and determined the method of defuzzification. The genetic algorithm double-optimized fuzzy PID control algorithm was designed to avoid the limitation of expert experience on the performance of analog PID control.Take the three characteristic spectral curve trends of 2500K, 5000K, and 10000K color temperatures as examples, the optimized fuzzy rules and affiliation functions were obtained iteratively, and the absolute color temperature spectral simulation experiments and AM1.5 solar spectrum simulation experiments were carried out on this basis. The results indicated that:

(1) The maximum single-point long spectral simulation errors of 2500K, 5000K, and 10000K color temperatures are −2.8%, 2.93%, and 2.76%, respectively, and the corresponding wavelengths are 556nm, 697.5nm, and 424.5, respectively, and the spectral curve area simulation errors are 0.18%, 0.22%, and 0.02%, respectively. There is no significant correlation between the stellar spectral simulation method based on the genetic algorithm and fuzzy PID composite control and the trend of the spectral curves.

(2) The simulation error of 2500K-10000K single-point spectrum was between −2.91% and 2.94%, and the simulation error of spectral curve area was between −0.18% and 0.22%, which indicated that the composite control spectral simulation algorithm based on genetic algorithm and fuzzy PID had good simulation effect in the absolute color temperature range of 2500K-10000K.

(3) The maximum single-point spectral simulation error of AM1.5 solar spectrum was -5.76%, which was larger than

the single-point spectral simulation error of absolute color temperature spectral simulation, and the spectral curve area simulation error was 0.07%, which was comparable to the spectral curve area simulation error of absolute color temperature spectral simulation, indicating that the composite control spectral simulation algorithm based on genetic algorithm and fuzzy PID is applicable to still have good performance in the case of less demanding spectral feature peak simulation.

In this paper, the composite control spectral simulation method based on a genetic algorithm and fuzzy PID had a high spectral simulation accuracy and at the same time, manifested excellent generalization in the spectral simulation of multi-color temperature and multi-target, along with a certain ability to simulate spectral detail features, which can provide the theoretical basis and technical support for high-precision multiple color temperature arbitrary modulation.

REFERENCES

[1] J. Liu, L. Wang, X. Li, C. Yu, H. Zhong, S. Liang, J. Yang, X. Lu, and M. Yang, "Star extraction based on clustering within a star tracker," *Scientia Sinica Technologica*, vol. 45, no. 3, pp. 257–262, Mar. 2015, doi: 10.1360/n092014-00480.

[2] D. Wang, J. Li, T. Dong, and D. Ge, "Multi-source fusion autonomous navigation technology based on spacecraft observability theory," *Sci. Technol. Foresinht*, vol. 1, pp. 146–158, Jan. 2022, doi: 10.3981/j.issn.2097-0781.2022.01.012.

[3] X. Ning and J. Fang, "On the observability of spacecraft navigation using landmarks," *J. Beijing Univ. Aeronaut. Astronaut.*, vol. 31, no. 6, pp. 673–677, 2005, doi: 10.3969/j.issn.1001-5965.2005.06.017.

[4] S. W. Brown, "LED-based spectrally tunable source for radiometric, photometric, and colorimetric applications," *Opt. Eng.*, vol. 44, no. 11, Nov. 2005, Art. no. 111309, doi: 10.1117/1.2127952.

[5] E. H. Miller, "A note on reflector arrays," *IEEE Trans. Antennas Propag.*, vol. 15, no. 5, pp. 692–693, Sep. 1967, doi: 10.1109/TAP.1967.1139012.

[6] X. Guang-Qiang, H. Y. Yu, J. H. Zhang, G. Y. Cao, L. Han, D. S. Li, and J. J. Yu, "Solar spectrum matching based on white LED compensated with monochromatic LEDs," *Chin. J. Lumin.*, vol. 38, no. 8, pp. 1117–1124, 2017, doi: 10.3788/fgxb20173808.1117.

[7] J. H. Davis and J. R. Cogdell, "Calibration program for the 16-foot antenna," Elect. Eng. Res. Lab., Univ. Texas, Austin, TX, USA, Tech. Rep., NGL-006-69-3, Nov. 1987.

[8] S. W. Brown, R. D. Saunders, Z. Li, A. Fein, and R. A. Barnes, "An absolute detector-based spectral radiance source," in *Proc. SPIE*, vol. 7807, pp. 65–73, Aug. 2010, doi: 10.1117/12.860544.

[9] D. Luo, S. Bauer, M. Taphanel, T. Langle, F. P. Leon, and J. Beyerer, "Optical unmixing using programmable spectral source based on DMD," in *Proc. SPIE*, vol. 9855, pp. 138–146, May 2016, doi: 10.1117/12.2228303.

[10] X. Wang and Z. Li, "A spectrally tunable calibration source using Ebert–Fastie configuration," *Meas. Sci. Technol.*, vol. 29, no. 3, Feb. 2018, Art. no. 035903, doi: 10.1088/1361-6501/aa9e31.

[11] D. Xu, G. Sun, G. Zhang, Y. Zhang, L. Wang, S. Liu, J. Zhong, S. Liang, and J. Yang, "Design of a digital tunable stellar spectrum calibration source based on a digital micromirror device," *Measurement*, vol. 191, Mar. 2022, Art. no. 110651, doi: 10.1016/j.measurement.2021.110651.

[12] L. Jing, "Spectral simulation method for calibration light source of transmissive visibility meter," *Acta Optica Sinica*, vol. 42, no. 6, 2022, Art. no. 0601005, doi: 10.3788/aos202242.0601005.

[13] S. Jiliang, "Spectral simulation method for calibrating light source of atmospheric transmissiometer based on digital micromirror," *Chin. J. Lasers*, vol. 49, no. 11, 2022, Art. no. 1111001, doi: 10.3788/cjl202249.1111001.

[14] W. Hongmin, T. Fan, and X. Ping, "A solar spectrum synthesis method based on monochrome LED," *Laser Optoelectron. Prog.*, vol. 57, no. 9, 2020, Art. no. 093004, doi: 10.3788/lop57.093004.

[15] C. Zhen, "LED spectrum matching based on adaptive differential evolution algorithm," *Acta Optica Sinica*, vol. 42, no. 9, 2022, Art. no. 0930004, doi: 10.3788/aos202242.0930004.

[16] X. Da, Z. Guo-Yu, S. Gao-Fei, Z. Yu, L. Jie, and M. Yi-Yuan, "Optical system design of star simulator light source with spectrum adjustable based on DMD," *Acta Photonica Sinica*, vol. 46, no. 7, 2017, Art. no. 722002, doi: 10.3788/gzxb20174607.0722002.

[17] H. X. Liu, L. Zheng, L. Dai, and M. Huang, "Research on the color calculation method of LCD based on the spectral radiation," *Appl. Mech. Mater.*, vols. 130–134, pp. 2977–2980, Oct. 2011, doi: 10.4028/www.scientific.net/amm.130-134.2977.

[18] Y. Yang, B. Hu, L. Li, S. Wang, and Q. Yan, "Design of MWIR Hadamard coded imaging spectrometer," *Opt. Precis. Eng.*, vol. 30, no. 6, pp. 641–650, 2022, doi: 10.37188/ope.20223006.0641.

[19] W. Huang, W. Zhang, and L. Weng, "Measurement and optimization control of output characteristics of high frequency magnetostrictive transducer," *Opt. Precis. Eng.*, vol. 30, no. 22, pp. 2876–2888, 2022, doi: 10.37188/ope.20223022.2876.

[20] X. Bao-Teng, Y. Xi-Bin, L. Jia-Lin, Z. Wei, T. Hao-Ran, and X. Da-Xi, "Image correction for high speed scanning confocal laser endomicroscopy," *Opt. Precis. Eng.*, vol. 28, no. 1, pp. 60–68, 2020, doi: 10.3788/OPE.20202801.0060.

[21] C. J. Harris, C. G. Moore, and M. Brown, *An Introduction to Intelligent Control*. 1993.

[22] O. Xinchuan, Y. Bowen, W. Jinyin, X. Ling, and C. Huadong, "Self-adaptive laser power stabilization system based on fuzzy control," *Chin. J. Lasers*, vol. 48, no. 1, 2021, Art. no. 0101003, doi: 10.3788/cjl202148.0101003.

YU ZHANG received the B.E. and M.S. degrees from the Changchun University of Science and Technology, Jilin, China, in 2012 and 2019, respectively, where he is currently pursuing the Ph.D. degree. His research interests include optical system testing and mounting technology.

YUEGANG FU received the bachelor's degree from the Changchun Institute of Optics and Precision Machinery, in 1995, and the master's and Ph.D. degrees in engineering from the Changchun University of Science and Technology, Jilin, China, in 2002 and 2005, respectively. He is currently the Vice President of the Changchun University of Science and Technology. His research interests include optical design and bionic optics.

QIANG LIU received the bachelor's degree from the College of Electronic Information, Changchun University of Science and Technology, Jilin, China, in 2020. He is currently pursuing the master's degree with the College of Optoelectronic Engineering, Changchun University of Science and Technology. His research interests include optical design and spectral simulation.

BIN ZHAO received the B.E. and M.S. degrees from the Changchun University of Science and Technology, Jilin, China, in 2012 and 2015, respectively, where he is currently pursuing the Ph.D. degree. His research interest includes remote-sensing calibration for spacecraft ground inspection.

JIAN ZHANG received the B.E. and M.E. degrees from the Changchun University of Science and Technology, Jilin, China, in 2012 and 2017, respectively. He is currently an Assistant Researcher with the School of Optoelectronic Engineering, Changchun University of Science and Technology. His research interests include aspects of meteorological instrument design, detection, and calibration of optoelectronic instruments.

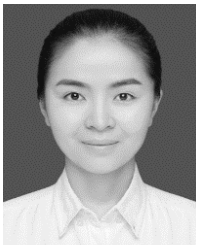

GAOFEI SUN received the B.E. degree from the Xi'an University of Technology, in 2008, and the M.E. degree from the Changchun University of Technology, Jilin, China, in 2013. She is currently with the College of Optoelectronic Engineering, Changchun University of Science and Technology. Her research interests include instrumentation science and technology.

SHITONG LIANG received the Ph.D. degree in engineering from XIT, in 2011. He is currently with the Beijing Institute of Control Engineering, Beijing, China. His research interests include optical design and astronomy.

LI WANG received the M.S. degree in engineering from Northwestern Polytechnical University, in 2001, and the Ph.D. degree in engineering from Xi'an Polytechnic University, in 2003. He is currently with the Beijing Institute of Control Engineering, Beijing, China. His research interest includes control technology.

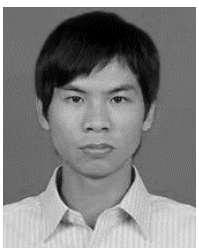

JUN ZHONG received the B.E. degree from the Nanjing University of Technology, in 2008, and the M.E. degree from the Changchun Institute of Optics and Mechanics, Chinese Academy of Sciences, in 2010. He is currently with the Beijing Institute of Control Engineering, Beijing, China. His research interests include system design of imaging optical systems and optical inspection.